PHYSICAL REVIEW A **95**, 011603(R) (2017)

Precise measurements on a quantum phase transition in antiferromagnetic spinor Bose-Einstein condensates

A. Vinit and C. Raman*

School of Physics, Georgia Institute of Technology, Atlanta, Georgia 30332, USA

(Received 23 October 2016; published 23 January 2017)

We have experimentally investigated the quench dynamics of antiferromagnetic spinor Bose-Einstein condensates in the vicinity of a zero temperature quantum phase transition at zero quadratic Zeeman shift q. The rate of instability shows good agreement with predictions based upon solutions to the Bogoliubov–de Gennes equations. A key feature of this work was removal of magnetic field inhomogeneities, resulting in a steep change in behavior near the transition point. The quadratic Zeeman shift at the transition point was resolved to 250 mHz uncertainty, equivalent to an energy resolution of $k_B \times$ (12 pK). A small (2–3 σ) shift of the transition point was observed, from $q = 0$ to $q = +650$ mHz, whose physical mechanism is currently unknown. In this work, we demonstrate a sub-Hz precision measurement of a phase transition in quantum gases. It paves the way toward observing shifts of the transition point due to finite particle number N that scale as $1/N$, and also to potential Heisenberg limited spectroscopy with antiferromagnetic spinor gases [L.-N. Wu and L. You, Phys. Rev. A **93**, 033608 (2016)].

DOI: 10.1103/PhysRevA.95.011603

Phase transitions are singular points in the behavior of many-body systems. In the real world, however, the mathematical singularity of a phase transition is usually hidden by heterogeneity. For example, in the domain of superfluids, gravity smears out the spectacular lambda point of liquid helium, requiring that precise comparisons of experiment and theory be performed in space [1]. For quantum gases of ultracold atoms the trap itself causes density variations that are intrinsic to the system [2]. For example, in a Bose-Einstein condensate (BEC) the particle density varies by 100% from the center to the edge of the Thomas-Fermi volume. A phase transition whose order parameter is proportional to the chemical potential will therefore be smoothed out, typically by $k_B \times$ (100–300 nK). This problem confounds the ability to observe and quantify critical behavior [3], as well as transition point shifts caused by many-body effects, including critical fluctuations [4]. While local measurements on optical lattices in two dimensions [5,6] have made great strides in alleviating the inhomogeneity problem, they are specialized geometries, and do not readily lend themselves to bulk quantum matter in three dimensions.

In this paper we report precise measurements of a quantum phase transition in a bulk spinor Bose-Einstein condensate. Being a first-order transition, it does not depend on the particle density or chemical potential and is therefore by nature immune to density variations [7–10]. We have located this transition point with unprecedented frequency uncertainties of 130 and 220 mHz due to statistical and systematic effects, respectively. The combined error in energy units is $k_B \times$ (12 pK). Here, we present a sub-Hz observation of a phase transition in quantum gases. Other spinor experiments have probed similar energy scales outside of a phase transition [11].

Once density inhomogeneities are removed, only finite size effects remain, that are $\propto 1/N$, and which disappear once the thermodynamic limit, $N \to \infty$, is taken. Finite size effects are manifest in "bottom-up" approaches to quantum simulation that utilize small particle numbers $N = 1 - 10$ [12,13]. However, a higher energy resolution alleviates the need to detect such small numbers of atoms and thus facilitates the observation of finite size effects. For example, at a resolution of $h \times$ (100 mHz) for our system, we estimate that they can be visible for N as large as 1000, which is within reach. Thus precise measurements of the kind explored here can realize a "top-down" approach to quantum simulation. Finite particle number magnifies quantum correlations and entanglement [14], and recent work has explored the possibility of ultraprecise, Heisenberg-limited spectroscopy using this phase transition [15].

Spinor BECs offer a rich phase diagram due to the interplay of magnetic fields and magnetic interactions [16–24]. The transition we examine is between polar and antiferromagnetic spin states in a spin-1 ^{23}Na BEC at a quadratic Zeeman shift $q = 0$ (see Fig. 1). In the current work we expand upon earlier observations [7,25] to make precise measurements of this phase transition. A key factor enabling the enhanced precision reported here is the application of magnetic fields parallel, rather than perpendicular, to the long axis of the cigar-shaped BEC. This has afforded us a tool to control and to explore the role played by magnetic field gradients in the quench dynamics. Our data provide a powerful argument that these gradients were responsible for smearing out the phase boundary observed in earlier work [7]. We argue that this arises from a decoherence mechanism inhibiting the production of spin pairs that tends to slow down the instability. By removing the field gradient, we have measured an instability rate that is in good agreement with Bogoliubov theory, thus resolving discrepancies noted earlier [7]. An important theme of our work is the use of *dynamics* to probe the phase transition boundaries, rather than attempting to reach the ground state through thermal equilibration, as other studies have done [16,20].

Our starting point is the spin-dependent mean-field Hamiltonian for spin $F = 1$ Bose-Einstein condensates in the low-

*chandra.raman@physics.gatech.edu

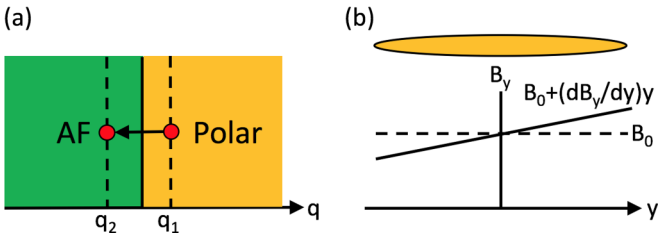

FIG. 1. Precise probe of quench dynamics in an antiferromagnetic spinor BEC. (a) Instantaneous quench of quadratic Zeeman shift from $q_1 > 0$ to $q_2 < 0$ through the quantum phase transition at $q = 0$ is performed using an AC (microwave) magnetic field. (b) DC magnetic field, kept constant during the experiment, consists of an applied bias field $\vec{B}$ that slowly varies in space, shown for fields applied along the long axis of the cigar-shaped condensate.

energy spin sector, as written in Ref. [7], with an additional, linear Zeeman term (see [9]):

$$H_{sp} = \frac{c_2}{2} n(\mathbf{r}) \langle \hat{\mathbf{F}} \rangle^2 + p(\mathbf{r}) \langle \hat{F}_z \rangle + q \langle \hat{F}_z^2 \rangle \qquad (1)$$

For the low values of p we are considering, the linear Zeeman term does not influence the overall density profile. $\hat{\mathbf{F}}, \hat{F}_z$ are the vector spin-1 operator and its z projection, respectively, and n is the particle density. For sodium atoms, the spin-dependent interaction coefficient $c_2 = \frac{4\pi\hbar^2}{3M}(a_2 - a_0) = +1.6 \times 10^{-52}$ J/m$^3 > 0$ [19], and hence the system is antiferromagnetic. Here M is the atomic mass, and $a_{2,0}$ are the scattering lengths for atom pairs whose total angular momentum $F_{\text{tot}} = 2$ and 0, respectively.

In our experiment, we controlled the linear Zeeman term through the spatial gradient of the magnetic field [see Fig. 1(b)], i.e., $p(\mathbf{r}) = g_F \mu_B (B_0 + \nabla B \cdot \mathbf{r})$, where $g_F = 1/2$ and μ_B are the Lande g factor and Bohr magneton, respectively. We controlled the quadratic Zeeman shift $q = \tilde{q} B_0^2 + q_M$ through a combination of static (DC) and microwave (AC) magnetic fields. Here B_0 is the DC magnetic field at the trap center, and $\tilde{q} = h \times 276$ Hz/G^2 is the coefficient of the DC quadratic shift for sodium atoms [8]. As in our earlier works, q_M is proportional to the microwave magnetic field strength through the AC Zeeman shifts of the $F = 1, m_F$ sublevels [7,25]. The microwave frequency was tuned below the "clock" transition, $|F = 1, m_F = 0\rangle \rightarrow |F = 2, m_F = 0\rangle$ at 1.772 GHz [26], by an amount between 260 to 470 kHz.

For a perfectly homogeneous magnetic field, we may apply a gauge transformation to the Hamiltonian to set $p = 0$ [9]. In this case, for an antiferromagnetic spinor BEC prepared in an initial state with zero net magnetization, as in our experiments, the ground state for $q > 0$ is a polar condensate consisting of a single component—the $m_F = 0$ spin projection that minimizes $\langle \hat{F}_z^2 \rangle$. For $q < 0$ the ground state maximizes the same quantity through a superposition of two components $m_F = \pm 1$, a so-called antiferromagnetic phase [27]. The symmetry properties of the ground state therefore change discontinuously at $q = 0$, defining a zero-temperature quantum phase transition [7,27].

Optically confined, cigar-shaped Bose-Einstein condensates in the $m_F = 0$ state were prepared in a static magnetic field aligned with one of the coordinate axes $i = x, y, z$ depicted in Fig. 1, which corresponds to the quantization axis in Eq. (1). The protocol is described in our earlier work [7]. Axial Thomas-Fermi radius and trap frequency were measured to be $R_y = 350$ μm and $\omega_y = 2\pi \times 7$ Hz, respectively. From these we determined the peak spin-dependent interaction energy, $c_2 n_0 = h \times 110$ Hz, accurate to about 10%. From the known trap aspect ratio of 70, we estimated the radial Thomas-Fermi radius to be $R_\perp = 5$ μm. For the data studied here very close to the phase transition point, there is insufficient energy for transverse excitations, whose threshold we estimate to be $> h \times 50$ Hz from a box model [28]. Thus only axial spin domains could form. The measured temperature was 400 nK, close to the chemical potential of 340 nK. The number of condensed atoms was approximately $N_c = 5 \times 10^6$.

We rapidly switched q from $q_1 > 0$ to a final value $q_2 < 0$ at $t = 0$ by changing only the AC magnetic field, keeping the DC magnetic field constant. Following a variable hold time, we switched off the trap and used time-of-flight Stern-Gerlach (TOF-SG) observations to record the one-dimensional (1D) spatiotemporal pattern formation in each of the three spin components, $n_i(y)$, $i = 0, \pm 1$, with a resolution of 10 μm. For the current work we focus on the total population in each of the spin states, $N_i = \int n_i(y) dy$, as well as the population fractions $f_i = N_i / \sum_j N_j$.

To control magnetic bias fields during the previously described experimental sequence, we used three pairs of orthogonal Helmholtz coils wrapped around the vacuum chamber. For a bias along $\hat{x}_j$, $j = 1,2,3$, we eliminated fields transverse to the x_j axis with two pairs of coils, after which we applied a constant current along the x_j axis. The actual magnetic field magnitude $|B|$ at the location of the atoms was determined via microwave spectroscopy of the $F = 1$, $m_F = 0 \rightarrow F = 2$, $m_F = \pm 1$ transitions through their Zeeman frequency shift of $g_F \mu_B |B|/h = 700$ kHz/G relative to the previously mentioned clock transition. In addition to these bias coils, we used a single anti-Helmholtz coil pair aligned with the y axis to generate magnetic field gradients of up to 160 mG/cm in magnitude. Background field gradients along the y direction were observed to be in the neighborhood of 80 mG/cm. Our uncertainty in magnetic field calibration was 4 mG.

The gradient cancellation was achieved as follows. By tuning the field gradient coils, we noticed that, at $dB_y/dy = 0$, a pure mixture of $m_F = \pm 1$ states remained perfectly overlapped, whereas for $dB_y/dy < 0$ and $dB_y/dy > 0$ the two states phase separated by $\delta x < 0$ and $\delta x > 0$, respectively, in order to gain linear Zeeman energy [16]. Independent confirmation was provided by an initial $m_F = 0$ condensate at $q > 0$. This should be the ground state of the spinor Hamiltonian, but only at zero field gradient. For any finite gradient we observed a slow decay into a mixture of all three spin states, similar to results from the Ketterle group [16]. The field gradient null point also maximized the lifetime of the $m_F = 0$ state, which could be several seconds.

The finite current resolution of our power supply controls limited the resolution to ± 0.3 mG/cm. With this resolution the residual linear Zeeman energy p after cancellation of stray magnetic field gradients was no more than $\pm 7\%$ of the spin-dependent interaction energy U. A complementary technique for measuring field gradients with similar resolution to ours observed the formation of helical spin textures using Larmor precession imaging [29].

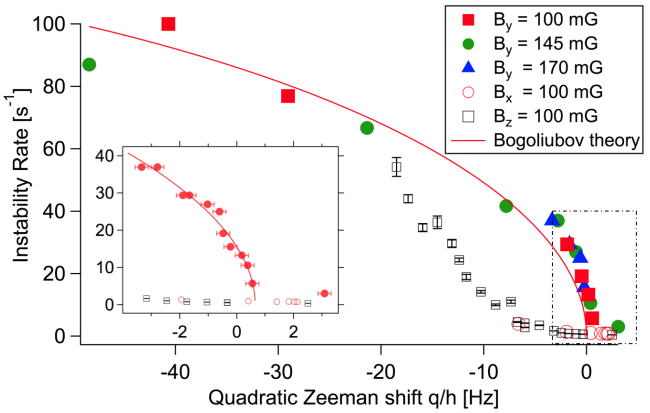

FIG. 2. Probing the phase transition with ∼100 mHz sensitivity. Solid symbols are data taken for different static magnetic fields B_y, i.e., along the cigar. Clear symbols were taken in the two transverse directions B_x, B_z. The solid line is a fit of all B_y data to the rate given by Bogoliubov theory for a homogeneous BEC, as described in the text. The inset is an expanded view of the data outlined in the dashed box, with solid circles for all B_y data. The solid line is a separate fit allowing for an offset q_0, measured to be $+0.65 \pm 0.13$ Hz. Vertical error bars are statistical, while horizontal error bars are uncertainty in q calibration of 0.22 Hz. B_z data are reprinted from [7].

Figure 2 shows our main experimental observation. It is the extreme sensitivity of the instability rate to quadratic Zeeman shift near the phase boundary, allowing for a precise determination of the latter. Similar to our earlier work [7,25], we measured the fractional population in $m_F = \pm 1$, i.e., $f_{\pm 1} = f_1 + f_{-1}$, which was observed to grow with time. The instability rate was defined to be $\Gamma_{1/2} = 1/T_{1/2}$, where $T_{1/2}$ was the time at which $f_{\pm 1}$ had increased to $1/2$. The extreme sensitivity was only observed for magnetic fields aligned parallel to the long axis of the cigar-shaped BEC (hereafter B_y), where we could carefully null stray magnetic field gradients. By contrast, we measured a stark difference for fields aligned along $B_{x,z}$. In this case, according to our earlier observations (data reproduced from [7] in Fig. 2 as open squares), a significant discrepancy was noticed between the experimentally observed instability rates and those predicted by Bogoliubov theory, particularly for data taken near the transition point. The experimental data suggested a smooth turn-on of the instability rate rather than a sharp transition point. In the current work we have reproduced this difference for magnetic fields B_x (open circles), which agrees with the previous B_z data. With the newer B_y data we observe a much closer agreement with the theoretical prediction for a homogeneous system, $\Gamma(q) = \sqrt{|q|(q + 2c_2 n_0)}$, the solid line in the figure. Here n_0 is the peak density of the $m_F = 0$ cloud. The theoretical line is a fit to the experimental data yielding $c_2 n_0 = h \times 125 \pm 11$ Hz, which agrees with the experimentally determined value within the quoted uncertainties.

Focusing now only on B_y data with the gradients canceled in Fig. 2, we applied three different magnetic fields $B_y =$ 100, 145, and 170 mG, and adjusted the microwave power accordingly to cover the same range of total quadratic Zeeman shift. In all three cases the data collapsed onto what appears to be a single curve, particularly for small q very close to the transition point. For larger static fields of 200 mG, the difference between transverse and longitudinal instability rates was less appreciable, for reasons that are not presently clear. It is possible that the larger microwave power required to cancel the increased quadratic shift caused a spin-state-dependent atom loss that suppressed the instability.

The inset to the figure shows an expanded view of the data outlined in the dashed box. Here, the data sets from different static fields have been combined into one. This data very close to the transition point were separately fit to a Bogoliubov function $\Gamma(q - q_0)$ that has been shifted empirically by q_0, yielding $q_0 = 0.65 \pm 0.13$ Hz. The quoted error is the statistical uncertainty in the fit to the first nine data points starting from the left in the inset. Although no physical theory motivates this choice of fitting function, it does provide a useful parametrization of our data, particularly the *steepness* with which it approaches $\Gamma = 0$ from the $q < 0$ side. The error bars along the q axis are the 200 mHz experimental uncertainty in determination of the $q = 0$ point due to the bias magnetic field calibration uncertainty of 4 mG. Other error sources, including microwave magnetic field amplitude and frequency uncertainties, were much smaller and could be neglected. A better magnetic field calibration could help reduce this uncertainty.

With this level of precision the data suggest a 2 to 3 σ shift of the phase transition point to $q = +650$ mHz. We do observe a finite instability rate of about 3 s^{-1} for $q = +3$ Hz, in the absence of any microwave fields. This could be caused by spin redistribution from background AC magnetic fields not measured by our magnetic field calibration technique, for which further study would be needed. Apart from this technical consideration, it is also possible that the transition point is shifted due to fundamental reasons, either interactions with the thermal cloud or, perhaps, to non-mean-field effects. We note that for $q > 0$, thermally induced distillation of atoms from $m_F = 0$ to $m_F = 1$ has been previously observed in elongated BECs, but only at much larger field gradients of 100 mG/cm [30]. It is not clear that the weak gradients here of < 0.3 mG/cm can cause this background instability. Notwithstanding these experimental caveats, the sub-Hz level precision spectroscopy of a phase transition has not been achieved previously in ultracold gases, to our knowledge.

While the data in Fig. 2 appear to have a universal character, we do not yet have a complete explanation why transverse fields appear to suppress the instability relative to longitudinal fields. We have evidence, however, that spatial inhomogeneities in the field magnitude play an important role, and we explore this effect in the rest of the paper. Since these gradients were different for transverse and longitudinal fields, this effect by itself might explain the observed differences.

To understand this point in further detail, we note that for a one-dimensional system we only need to consider variations in magnetic field along the y direction. Thus, for fields that are mostly B_y, the first-order magnetic field is given by $B = |\vec{B}| \approx B_0 + \frac{\partial B_y}{\partial y} y$, and by applying an external field gradient $-\frac{\partial B_y}{\partial y}$ we could cancel the field inhomogeneity to first order. For a bias field that is mostly B_z, the only term that is relevant in the same order is the variation of that field along y: $|\vec{B}| \approx B_0 + \frac{\partial B_z}{\partial y} y$, since all other gradient terms $\partial B_{y,x}/\partial y$ add in quadrature and

should be suppressed. A similar argument applies to fields that are mostly B_x. Transverse field gradients of this type could neither be easily characterized nor canceled using our current setup [31]. However, as noted earlier [7], they did appear to play some role in the problem, since at long times $t > 1$ s the cloud had separated into two distinct domains of $m_F = \pm 1$, consistent with a gradient in the linear Zeeman term. In the absence of a field gradient these two spin states would be miscible with one another.

An alternative and very intriguing explanation is a genuine orientation dependence of the instability upon the bias field. This would signal physics beyond a mean-field description of the spinor BEC, an exciting development. For example, dipolar interactions [32–34] have an anisotropy in space and can influence the spin relaxation rate for sufficiently anisotropic trapping potentials [35]. The similarity of the data in Fig. 2 for both B_x and B_z fields suggests this as a possibility, although the effect in Ref. [35] is unfortunately too weak to explain the factor-of-10 suppression observed. Without further study we hold dipolar effects in abeyance.

To separate out the role played by magnetic field gradients from other potential causes, we performed controlled experiments with the magnetic field applied along the y direction, and negligible z and x fields. Here the field gradient $B_p = \frac{\partial B_y}{\partial y}$ was *deliberately* applied, and could be tuned to both positive and negative values by varying the current in the anti-Helmholtz coils. Thus, to a good approximation we had independent control over p and q.

Figure 3 shows the variation of $\Gamma_{1/2}$ with applied magnetic field gradient, which has been normalized in order to compare with 1D numerical simulations. The normalized gradient is B_p/B_{p0}, where $B_{p0} = \frac{\hbar\omega_y}{g_F\mu_B a_y} \simeq 13$ mG/cm and ω_y and $a_y = \sqrt{\hbar/m\omega_y}$ are the axial frequency and oscillator length, respectively. The data clearly show that the maximum rate occurs near $B_p = 0$, and falls off rapidly with field gradient to either positive or to negative values. Due to nonidealities in the experiment, the gradient coils introduced an asymmetric bias field variation which was independently measured. For normalized field gradients < -3 this caused an increase in $|q|$ that created a small, positive deviation between the experimental data and the theory on the left side of the graph.

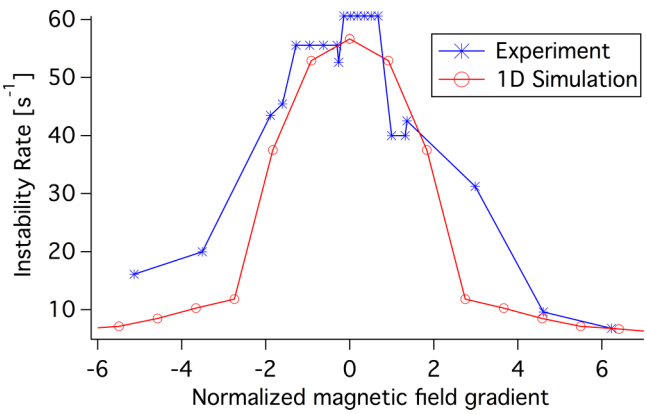

FIG. 3. Field gradient slows down the instability. Shown are experimentally measured and numerically computed instability rates versus applied magnetic field gradient. The quadratic shift was $q = -3.7$ Hz at zero field gradient, and varied from -5 to -2.5 Hz over the data range shown.

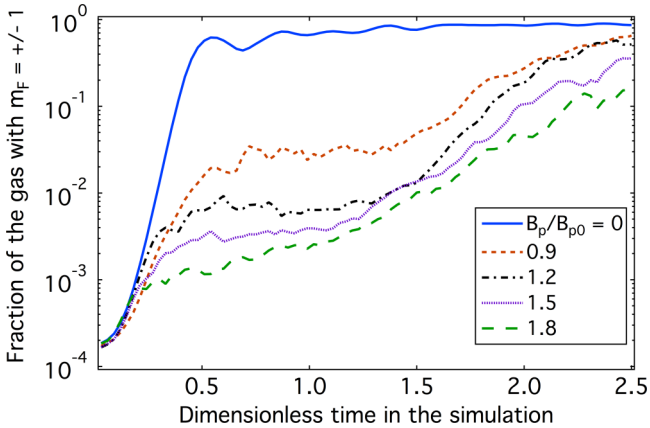

FIG. 4. Origin of field-gradient induced suppression of instability. Numerical simulations of the dynamical evolution of the $f_{\pm 1}$ populations for various field gradients show the formation of a plateau, as described in the text. The dimensionless time unit is $2\pi/\omega_y$.

Also plotted is the result of 1D numerical simulations based on the truncated Wigner approximation (TWA) [25]. These were performed for $B_p > 0$, and the results are reflected about the y axis in the figure for $B_p < 0$. These numerical data were scaled by a factor of 2 in both x and y axes, and show good agreement with our measured data. Although we cannot at present account for an overall scaling factor, we can account for the fact that it is the same for both x and y axes in the figure. This is due to the linearity of the Bogoliubov equations that describe the initial instability. All quantities of interest, including p, q, and the (imaginary) eigenvalues E, scale linearly with the chemical potential. If experiment and theory were performed at different values for μ, a single scaling factor should apply to the quantities plotted in both axes of Fig. 3. This argument should be approximately true even for larger hold times, provided that the system is still in the growth phase of the dynamics where nonlinearities are not too strong.

What causes the suppression? The numerically obtained wave functions show that noise in the initial state becomes amplified by the instability, forming localized domains that grow with time, as noted in earlier work [25]. Figure 4 shows numerical results for the temporal dynamics of the population $f_{\pm 1}$ for different values of the field gradient B_p, plotted in dimensionless time units $T_y = 2\pi\omega_y^{-1}$. For both $B_p = 0$ and $B_p \neq 0$, we observe rapid domain growth, but for $B_p \neq 0$ a plateau in $f_{\pm 1}$ is reached. The plateau value decreases with increasing field gradient, and is <0.01 for normalized field gradients $B_p/B_{p0} \gtrsim 1.0$. Further growth of the ± 1 populations must wait until a longer time $T_{\rm late} \sim 1.5$, which is the timescale observed in the experiment, i.e., $\Gamma_{1/2} > 1/T_{\rm late}$. By examining the numerically generated wave functions, we observed that near $t = T_{\rm late}$ the meagerly populated ± 1 domains had diffused to opposite sides of the trap where their population could increase more easily at the expense of the smaller $m_F = 0$ population near the Thomas-Fermi boundaries.

Our simulations therefore suggest that there are *two* stages to the dynamics: early ($t \ll T_{\rm late}$) and late ($t \sim T_{\rm late}$). In the early stage, a clamping of the initial $m_F = \pm 1$ population, rather than a reduction of the instability rate, occurs. This early stage is critical for slowing down the instability. Unfortunately, our current experimental sensitivity does not allow us to probe population fractions $f_{\pm 1} < 0.05$. We can, however, understand the numerical observations in terms of a decoherence process caused by the field gradient. In the presence of a magnetic field gradient, the quantum field operator, $\hat{\psi}_m$, acquires a phase gradient that increases with time: $\phi = mE_Z ty/\hbar$, where $E_Z = g_F \mu_B (dB/dy)$. If ϕ varies by 2π over a single domain, the effective rate of amplification can be reduced by destructive interference from different spatial regions. For a domain of size d this occurs when $\frac{B_p}{B_{p0}}(\frac{\omega_y t d}{a_y}) = \pi$. For $\omega_y = 2\pi \times 7\ {\rm s}^{-1}$, a domain size of 30 μm, and $\frac{B_p}{B_{p0}} = 1.2$, this occurs at 16 ms, which is a similar timescale to the instability itself (see data for $B_p = 0$ in Fig. 3). This picture is therefore consistent with the formation of a plateau early in the dynamical evolution, as seen in Fig. 4. Since the decoherence is a process local to individual domains, it should not depend on whether the overall density profile is homogeneous or inhomogeneous.

In conclusion, we have made sub-Hz level precise measurements of the location of a quantum phase transition by observing a dynamical instability. We achieved this through careful control of magnetic field gradients that revealed a new mechanism for suppression of the instability. We observed a small shift in the transition point from $q = 0$ to $q_0 = +0.65 \pm 0.13$ Hz, whose origin merits further study. Our observations pave the way toward realizing entangled states appearing at very small values of the quadratic shift, $q < c_2 n_0/N$ [14,36]. For our atom density, this equals 100 mHz at $N = 1000$, which should be quite feasible to detect.

We thank Mukund Vengalattore and Carlos Sá de Melo for useful conversations. This work was supported by NSF Grant No. 1100179.

[1] J. A. Lipa, J. A. Nissen, D. A. Stricker, D. R. Swanson, and T. C. P. Chui, Phys. Rev. B **68**, 174518 (2003).
[2] L. Pitaevskii and S. Stringari, *Bose-Einstein Condensation*, International Series of Monographs on Physics (Clarendon, Oxford, 2003).
[3] I. Bloch, J. Dalibard, and S. Nascimbene, Nat. Phys. **8**, 267 (2012).
[4] F. Gerbier, J. H. Thywissen, S. Richard, M. Hugbart, P. Bouyer, and A. Aspect, Phys. Rev. Lett. **92**, 030405 (2004).
[5] W. S. Bakr, A. Peng, M. E. Tai, R. Ma, J. Simon, J. I. Gillen, S. Folling, L. Pollet, and M. Greiner, Science **329**, 547 (2010).
[6] C. Weitenberg, M. Endres, J. F. Sherson, M. Cheneau, P. Schauss, T. Fukuhara, I. Bloch, and S. Kuhr, Nature (London) **471**, 319 (2011).
[7] E. M. Bookjans, A. Vinit, and C. Raman, Phys. Rev. Lett. **107**, 195306 (2011).
[8] M. Ueda, Annu. Rev. Condens. Matter Phys. **3**, 263 (2012).
[9] D. M. Stamper-Kurn and M. Ueda, Rev. Mod. Phys. **85**, 1191 (2013).
[10] N. T. Phuc, Y. Kawaguchi, and M. Ueda, Phys. Rev. A **88**, 043629 (2013).
[11] G. E. Marti, A. MacRae, R. Olf, S. Lourette, F. Fang, and D. M. Stamper-Kurn, Phys. Rev. Lett. **113**, 155302 (2014).
[12] S. Murmann, A. Bergschneider, V. M. Klinkhamer, G. Zürn, T. Lompe, and S. Jochim, Phys. Rev. Lett. **114**, 080402 (2015).
[13] S. Murmann, F. Deuretzbacher, G. Zürn, J. Bjerlin, S. M. Reimann, L. Santos, T. Lompe, and S. Jochim, Phys. Rev. Lett. **115**, 215301 (2015).
[14] X. Cui, Y. Wang, and F. Zhou, Phys. Rev. A **78**, 050701 (2008).
[15] L.-N. Wu and L. You, Phys. Rev. A **93**, 033608 (2016).
[16] J. Stenger, S. Inouye, D. M. Stamper-Kurn, H.-J. Miesner, A. P. Chikkatur, and W. Ketterle, Nature (London) **396**, 345 (1998).
[17] M. S. Chang, C. D. Hamley, M. D. Barrett, J. A. Sauer, K. M. Fortier, W. Zhang, L. You, and M. S. Chapman, Phys. Rev. Lett. **92**, 140403 (2004).
[18] L. E. Sadler, J. M. Higbie, S. R. Leslie, M. Vengalattore, and D. M. Stamper-Kurn, Nature (London) **443**, 312 (2006).
[19] A. T. Black, E. Gomez, L. D. Turner, S. Jung, and P. D. Lett, Phys. Rev. Lett. **99**, 070403 (2007).
[20] Y. Liu, S. Jung, S. E. Maxwell, L. D. Turner, E. Tiesinga, and P. D. Lett, Phys. Rev. Lett. **102**, 125301 (2009).
[21] C. Klempt, O. Topic, G. Gebreyesus, M. Scherer, T. Henninger, P. Hyllus, W. Ertmer, L. Santos, and J. J. Arlt, Phys. Rev. Lett. **103**, 195302 (2009).
[22] J. Kronjager, C. Becker, P. Soltan-Panahi, K. Bongs, and K. Sengstock, Phys. Rev. Lett. **105**, 090402 (2010).
[23] L. Zhao, J. Jiang, T. Tang, M. Webb, and Y. Liu, Phys. Rev. Lett. **114**, 225302 (2015).
[24] S. W. Seo, S. Kang, W. J. Kwon, and Y.-i. Shin, Phys. Rev. Lett. **115**, 015301 (2015).
[25] A. Vinit, E. M. Bookjans, C. A. R. Sá de Melo, and C. Raman, Phys. Rev. Lett. **110**, 165301 (2013).
[26] M. A. Kasevich, E. Riis, S. Chu, and R. G. DeVoe, Phys. Rev. Lett. **63**, 612 (1989).
[27] Y. Kawaguchi and M. Ueda, Phys. Rep. **520**, 253 (2012).
[28] M. Scherer, B. Lucke, G. Gebreyesus, O. Topic, F. Deuretzbacher, W. Ertmer, L. Santos, J. J. Arlt, and C. Klempt, Phys. Rev. Lett. **105**, 135302 (2010).
[29] M. Vengalattore, S. R. Leslie, J. Guzman, and D. M. Stamper-Kurn, Phys. Rev. Lett. **100**, 170403 (2008).
[30] H.-J. Miesner, D. M. Stamper-Kurn, J. Stenger, S. Inouye, A. P. Chikkatur, and W. Ketterle, Phys. Rev. Lett. **82**, 2228 (1999).
[31] This requires the installation of coils at an angle with respect to the principal $\hat{x}, \hat{y}, \hat{z}$ directions of our apparatus.
[32] B. Pasquiou, E. Maréchal, G. Bismut, P. Pedri, L. Vernac, O. Gorceix, and B. Laburthe-Tolra, Phys. Rev. Lett. **106**, 255303 (2011).
[33] Y. Eto, H. Saito, and T. Hirano, Phys. Rev. Lett. **112**, 185301 (2014).
[34] W. Zhang, S. Yi, M. S. Chapman, and J. Q. You, Phys. Rev. A **92**, 023615 (2015).
[35] F. Deuretzbacher, G. Gebreyesus, O. Topic, M. Scherer, B. Lucke, W. Ertmer, J. Arlt, C. Klempt, and L. Santos, Phys. Rev. A **82**, 053608 (2010).
[36] R. Barnett, J. D. Sau, and S. Das Sarma, Phys. Rev. A **82**, 031602 (2010).